Supporting Information

New Spinel Oxide Catalysts for Visible-Light-Driven Water Oxidation

*F. Conrad, M. Bauer, D. Sheptyakov, S. Weyeneth, D. Jaeger, K. Hametner, P.-E. Car, J. Patscheider, D. Günther, G. R. Patzke**

Table of Contents

Table S1. Experimental parameters of LA-ICP-MS investigations.

Parameter	**Value**
Laser type	ArF excimer
Laser wavelength	193 nm
Spot diameter (sample and standard)	60 μm
Repetition rate (sample and standard)	5 Hz
Laser energy density	9.3 J/cm^2
He carrier gas flow rate	1.1 L min^{-1}
RF power	1350
Nebulizer gas flow rate	0.84 L min^{-1}
Auxiliary gas flow rate	0.7 L min^{-1}
Coolant gas flow rate	17.5 L min^{-1}
Dwell time	10 ms
Detector mode	Dual (pulse and analog)

Data evaluation of X-ray absorption spectroscopy measurements.

Data evaluation started with background absorption removal from the experimental absorption spectrum by subtracting a Victoreen-type polynomial. To determine the smooth part of the spectrum, corrected for pre-edge absorption, a piecewise polynomial was used. It was adjusted in such a way that the low-R components of the resulting Fourier transform were minimal. After division of the background–subtracted spectrum by its smooth part, the photon energy was converted to photoelectron wave numbers k. The resulting χ(k)-function was weighted with k^3 and Fourier transformed using a Hanning window function. Data analysis was performed in k-space with Fourier filtered data according to the curved wave formalism of the EXCURV98 program with XALPHA phase and amplitude functions. The mean free path of the scattered electrons was calculated from the imaginary part of the potential (VPI set to –4.00 eV). An inner potential correction E_f was introduced when fitting experimental data with theoretical models that accounts for an overall phase shift between the experimental and calculated spectra. The amplitude reduction factor was determined by fitting a defined gallium oxide reference. To remove random noise, Fourier filtered spectra in the range of 1 – 4 Å (not phase corrected) were subjected to analysis, the number of independent parameters always being larger than the iterated ones.

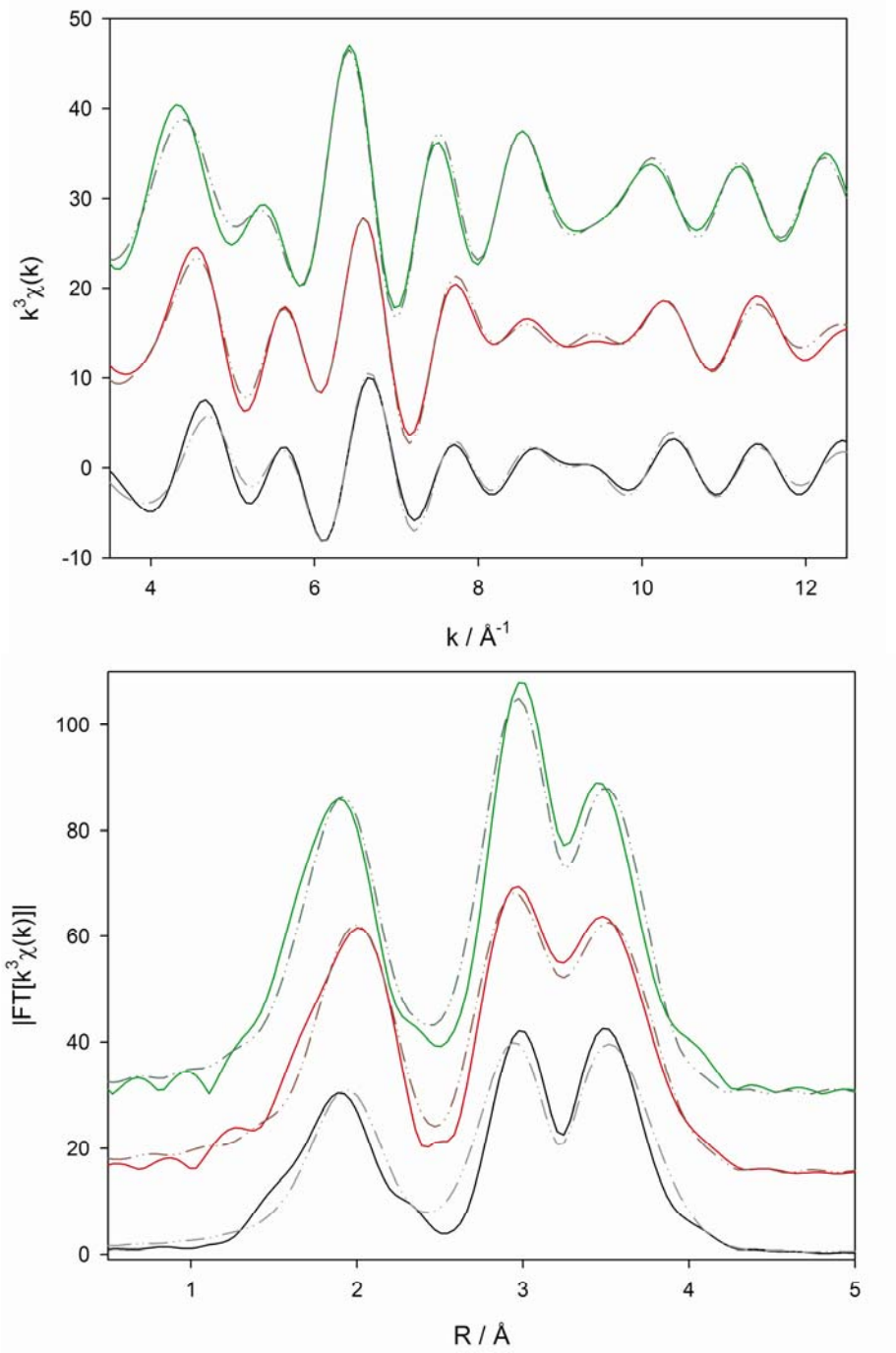

Figure S2. EXAFS spectra (top) of Co-Mn-Ga spinel, recorded at the Mn (black line), Co (red line) and Ga (green line) K-edge. The corresponding Fourier transformed functions are shown (bottom) as well as the theoretical spectra calculated according to the structural parameters given in Table S3.

Table S3. Results of the joint Rietveld refinement based on the neutron (HRPT, λ = 1.1545 Å) and X-ray ($Cu_{K\alpha1}$) powder diffraction data (S.G. *Fd3m*) for Co-Mn-Ga spinel. Soft constraints used: overall cation ratio in the sample: n(Mn)/n(Co)/n(Ga)=0.95/0.58/1.47 (derived from microprobe analyses).

***a*, Å**		8.3980(3)
site *8a* (1/8,1/8,1/8),	n(Mn)/n(Co)/n(Ga) (fractional)	0.417(15) / 0.238(35) / 0.346(21)
	B_{iso} (Å^2)	0.02(11)
site *16d* (1/2,1/2,1/2),	n(Mn)/n(Co)/n(Ga) (fractional)	0.267(8) / 0.17(2) / 0.563(11)
	B_{iso} (Å^2)	0.31(5)
site *32e* (*x*,*x*,*x*)	O	0.2599(1)
	B_{iso} (Å^2)	1.11(3)

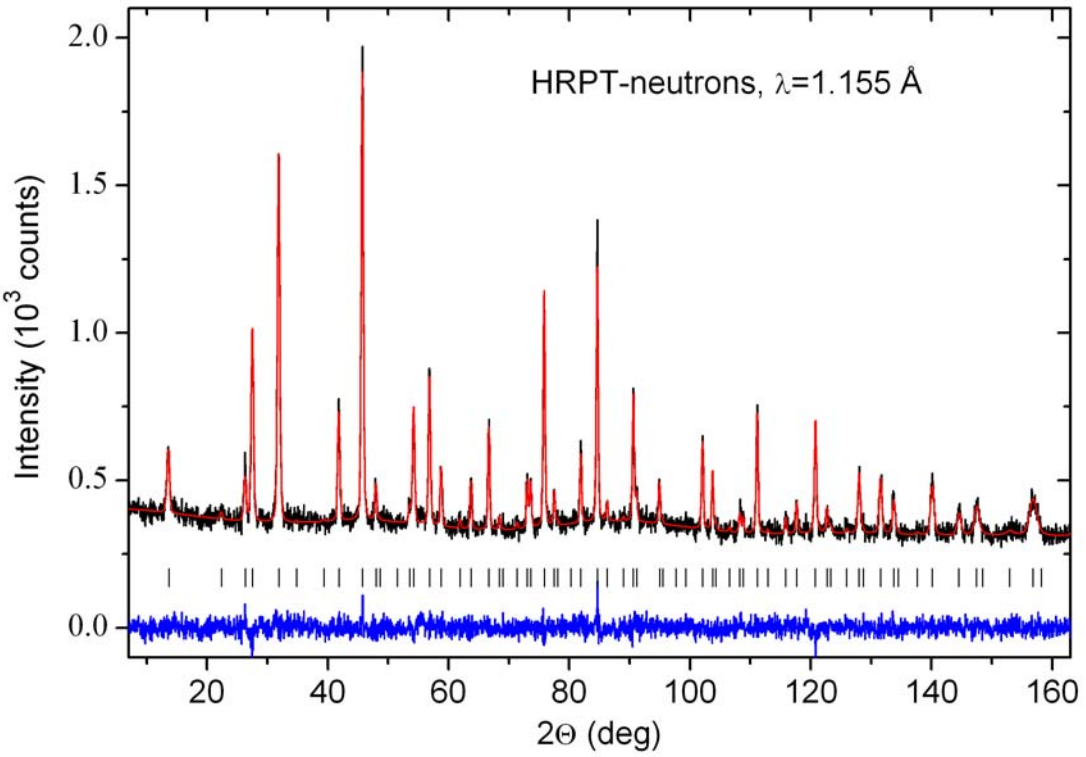

Figure S4. Rietveld refinement of the crystal structure parameters of Co-Mn-Ga spinel from neutron powder diffraction experiments. Experimental and calculated profiles, difference curves and peak position markers are shown.

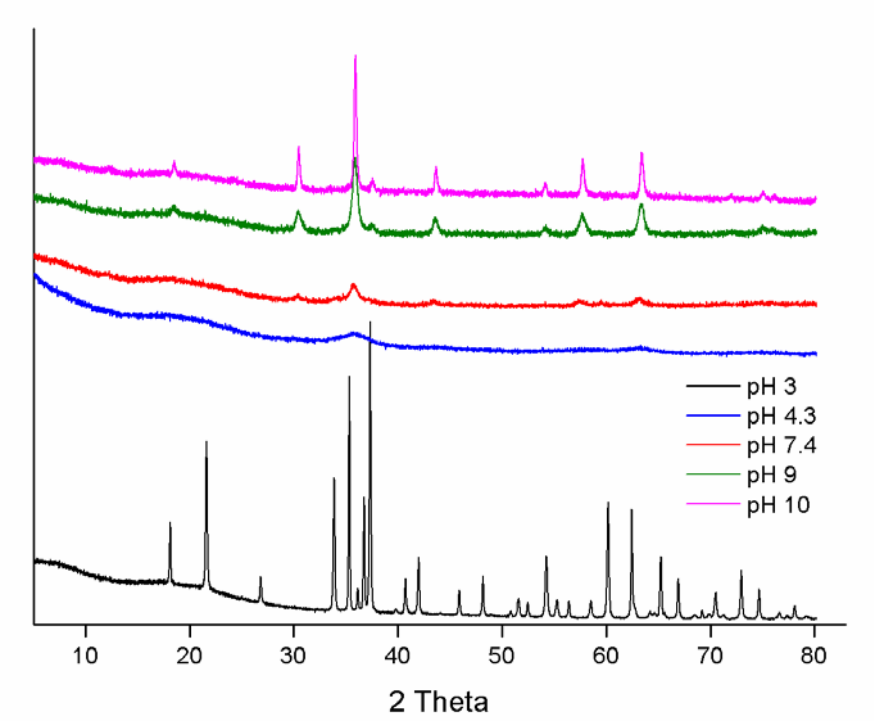

Figure S5. PXRD patterns monitoring the pH dependent microwave-hydrothermal formation of Co-Ga spinel. A GaOOH-related compound (cf. ICSD PDF 26-0674) is formed at low initial pH values (bottom, black) and the crystallinity of Co-Ga spinel (cf. ICSD PDF 11-0698) increases with the initial pH of the reaction system (upper colored patterns).

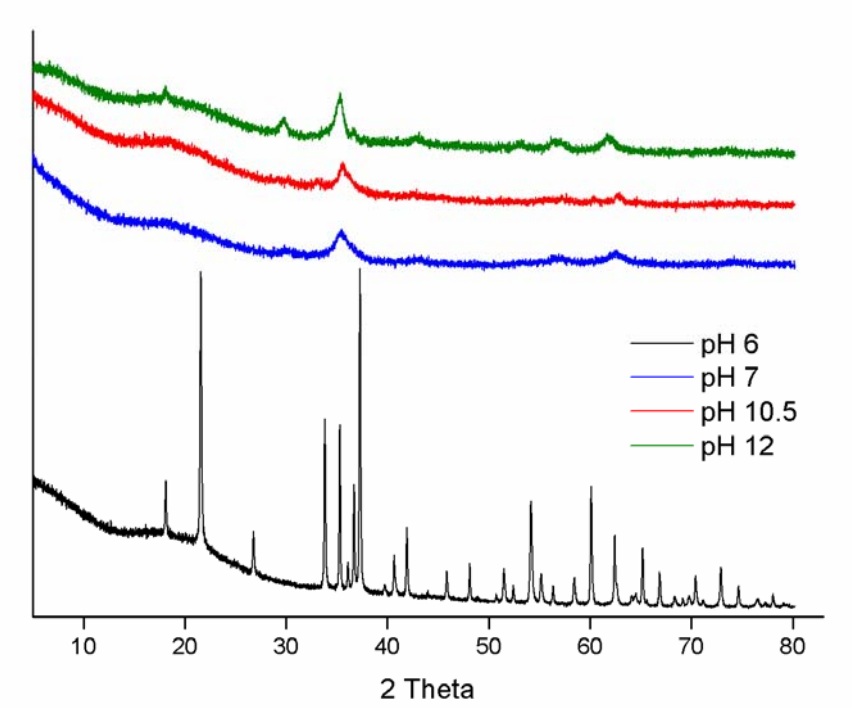

Figure S6. PXRD patterns monitoring the pH dependent microwave-hydrothermal formation of Mn-Ga spinel. A GaOOH-related compound (cf. ICSD PDF 26-0674) is formed at low initial pH values (bottom, black) and the crystallinity of Mn-Ga spinel (upper colored patterns) increases with the initial pH of the reaction system.

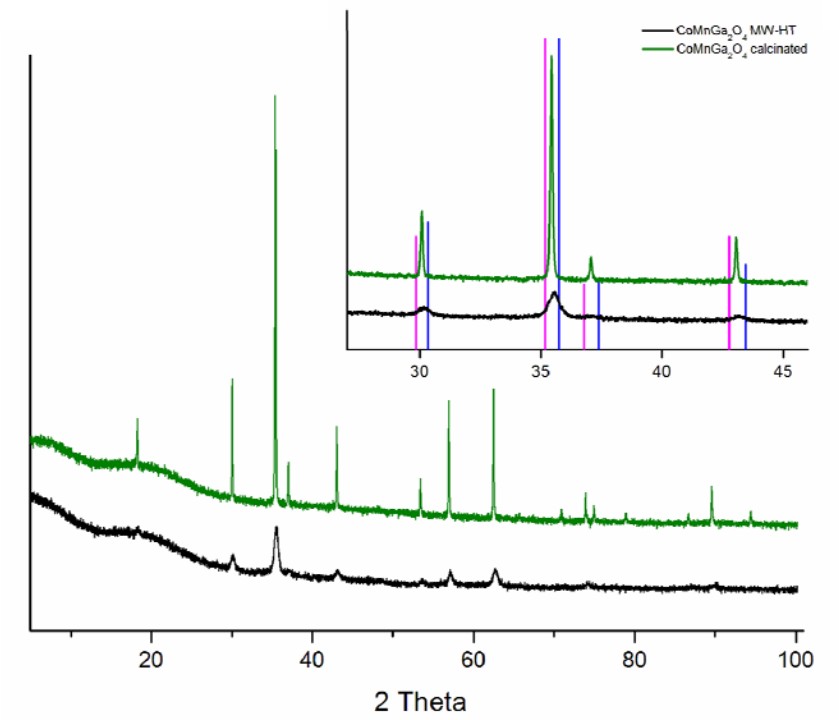

Figure S7. PXRD pattern of MW-HT synthesized Co-Mn-Ga spinel before (black) and after (green) calcination at 1050 °C in N_2 atmosphere; inset: comparison with literature data for $CoGa_2O_4$ (ICSD PDF 11-0698, blue) and $MnGa_2O_4$ (ICSD PDF 36-0181, pink). Calculated particle size of as-synthesized Co-Mn-Ga spinel according to the Scherrer equation: ca. 15 nm.

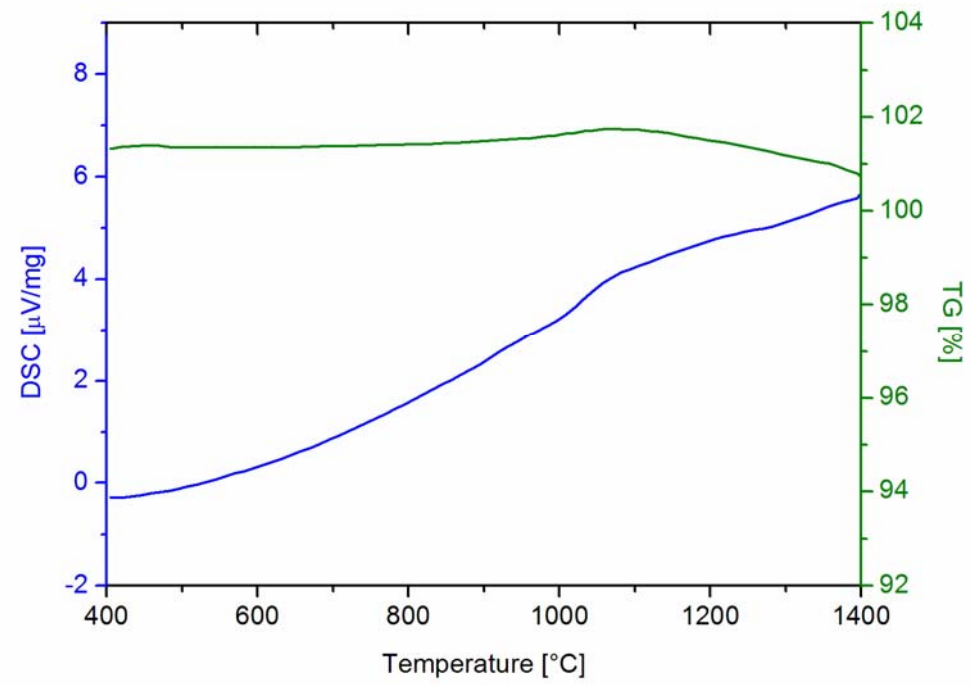

Figure S8. TG/DSC curve of Co-Mn-Ga spinel demonstrating thermal stability of the material up to 1400 °C (the appearing mass loss of ~0.5 % can be attributed to baseline fluctuations of the machine).

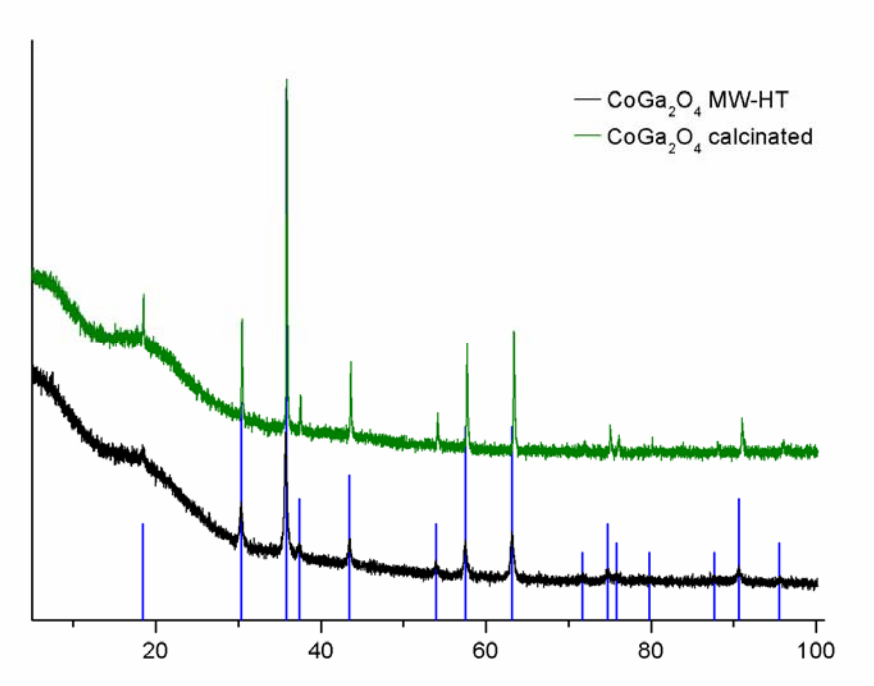

Figure S9. PXRD pattern of Co-Ga spinel synthesized via microwave-hydrothermal route (bottom: black pattern) and calcined at 900 °C (top: green pattern) vs. reference data (ICSD PDF 11-0698, blue). Calculated particle size of as-synthesized Co-Ga spinel according to the Scherrer equation: ca. 20 nm.

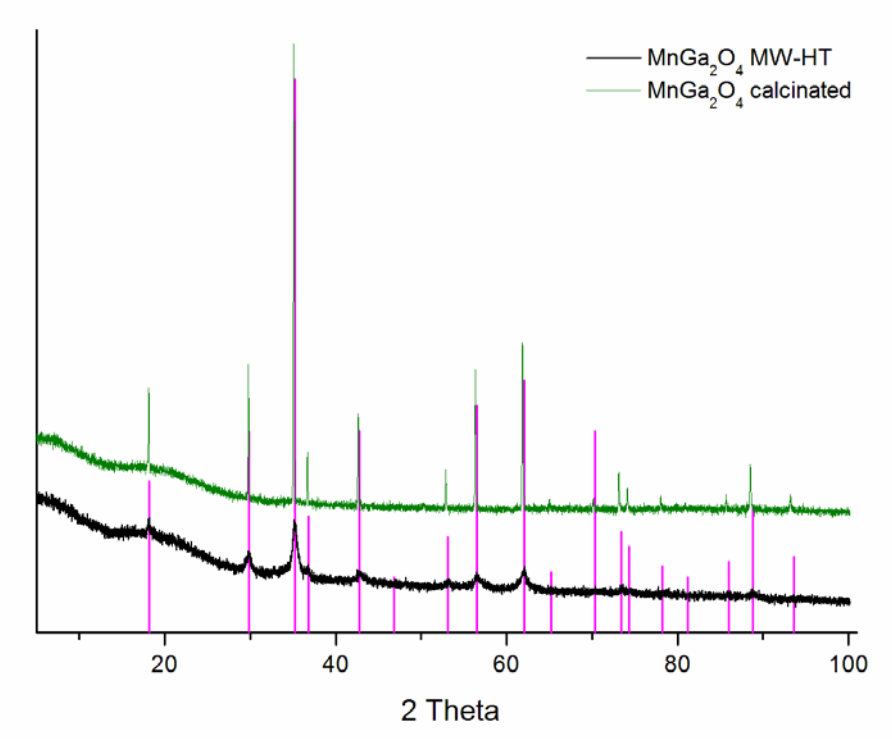

Figure S10. PXRD pattern of Mn-Ga spinel synthesized via microwave-hydrothermal route (bottom: black pattern) and calcined at 1000 °C (top: green pattern) vs. reference data for $MnGa_2O_4$ (ICSD PDF card 36-0181, pink). Calculated particle size of as-synthesized Mn-Ga spinel according to the Scherrer equation: ca. 15 nm.

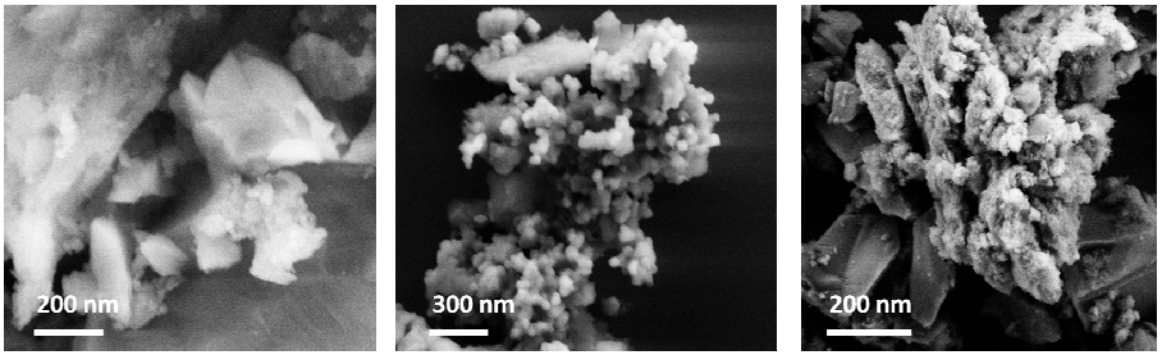

Figure S11. Representative SEM images of Mn-Ga spinel (left, calcined at 1000 °C; BET surface = 3.4 m^2/g), Co-Ga spinel (middle, calcined at 900 °C; BET surface = 7.5 m^2/g) and mixed Co-Mn-Ga spinel (right, after TG/DSC up to 1400 °C; BET surface = 6.8 m^2/g).

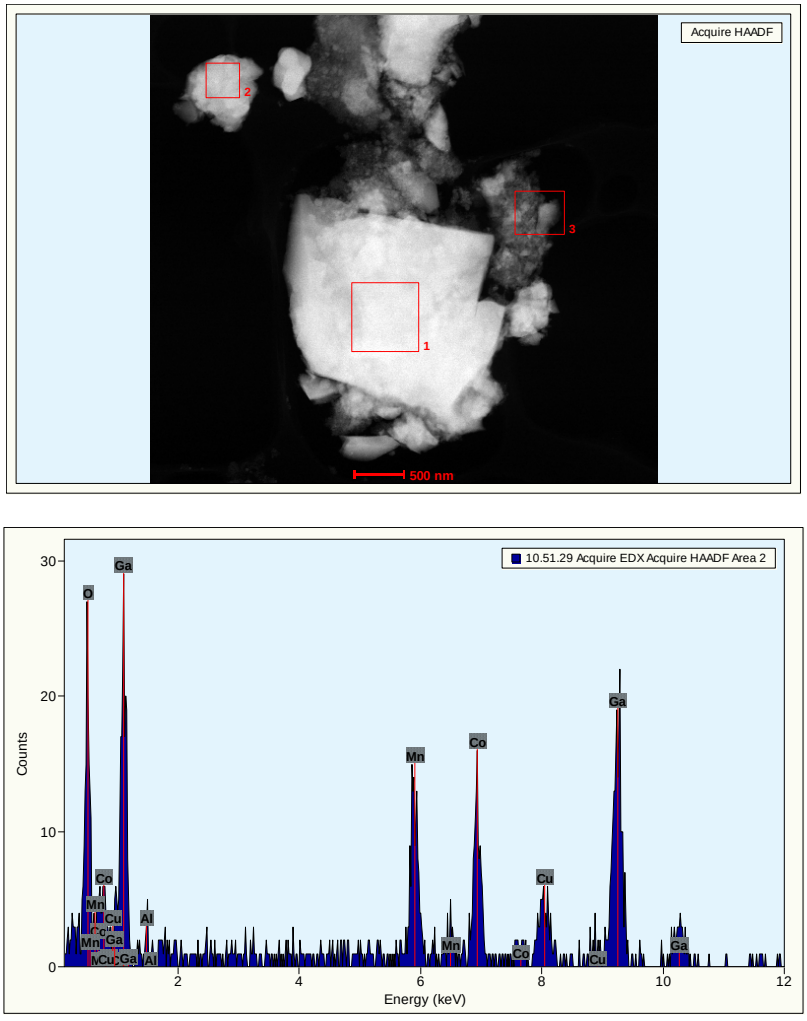

Figure S12. Representative STEM image (top; inset with spots indicating EDX analyses) and representative EDX spot analysis of calcined Co-Mn-Ga spinel (Cu signals arise from the sample holder).

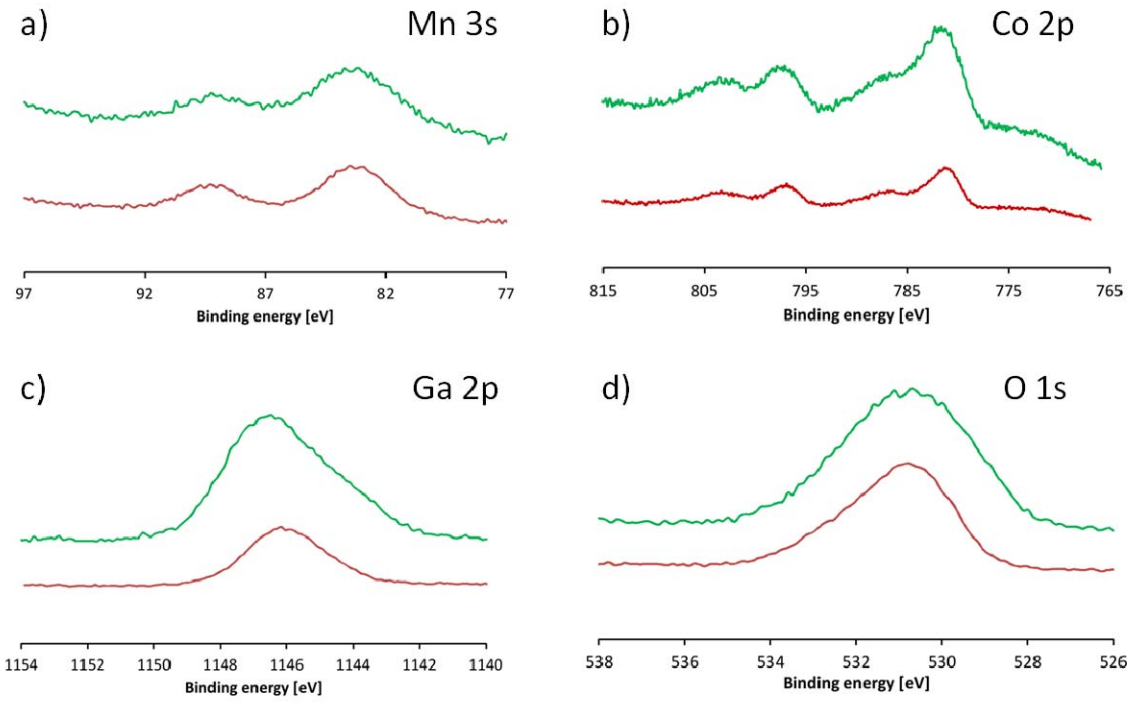

Figure S13. XPS spectra for calcined and as-synthesized Co-Mn-Ga spinel: (a) Mn 3s region, (b) Co 2p region, (c) Ga 2p region, (d) O 1s region.

Table S14. XPS peak positions (eV) of as-synthesized and calcined Co-Mn-Ga spinel in comparison with reference data.

Peak	**Co-Mn-Ga (as-synth.)**	**ΔMn [eV]**	**Co-Mn-Ga (calcined)**	**ΔMn [eV]**	**Reference data**				**Lit.**
					ΔMn				
Mn $3s_{1/2}$	83.2		83.1		**MnO**	**Mn_2O_3**	**Mn_3O_4**	**MnO_2**	
Mn $3s_{3/2}$	89.0	5.8	89.1	6.0	6.1	5.3	5.4	4.5	[1]
					MnO	**Mn_2O_3**	**Mn_3O_4**	**MnO_2**	
Mn $2p_{3/2}$	641.8		641.8		641.0	641.5	641.9	642.6	[1]
Mn $2p_{1/2}$	653.7		653.5		653.0	653.8			[2]

[1] V. di Castro and G. Polzonetti, *J. Electron Spectrosc. Rel. Phenom.*, 1989, **48**, 117.

[2] J. Töpfer, A. Feltz, D. Gräf, B. Hackl, L. Raupach and P. Weissbrodt, *Phys. Stat. Sol.*, 1992, **134**, 405.

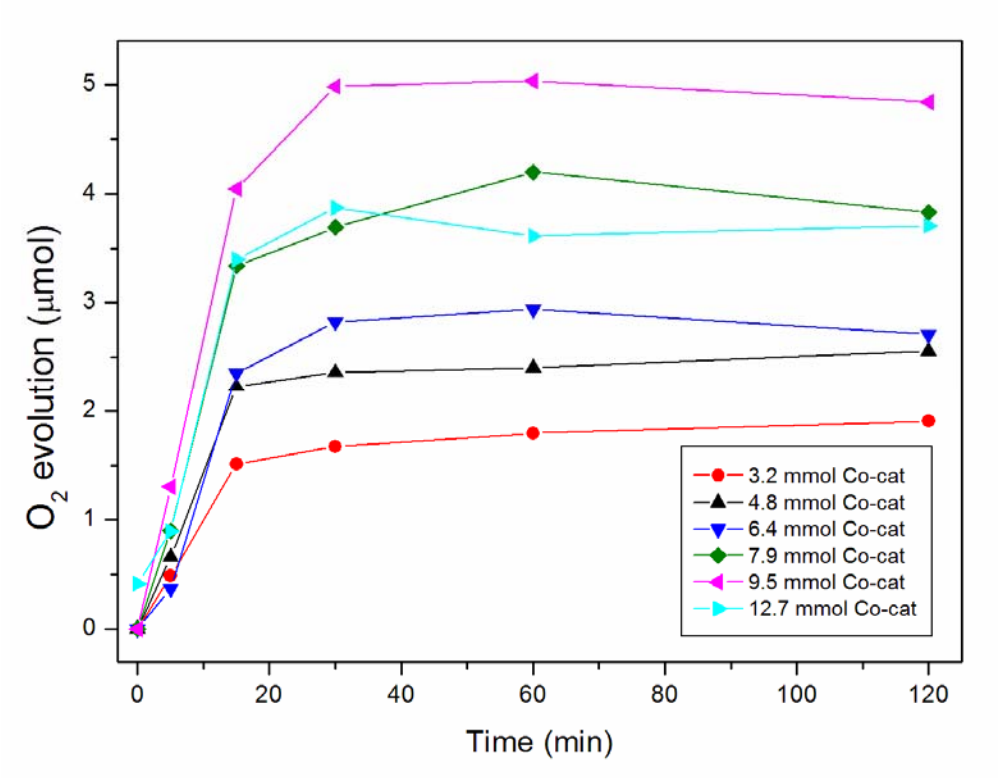

Figure S15. Concentration-dependent WOC activity of Co-Ga spinel.

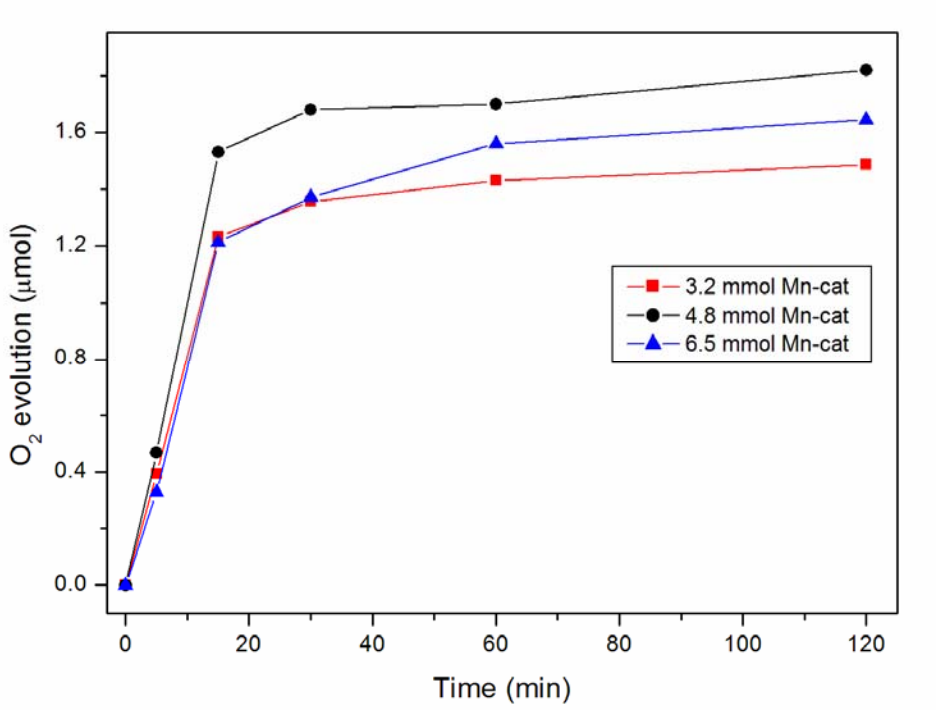

Figure S16. Concentration-dependent WOC activity of Mn-Ga spinel.

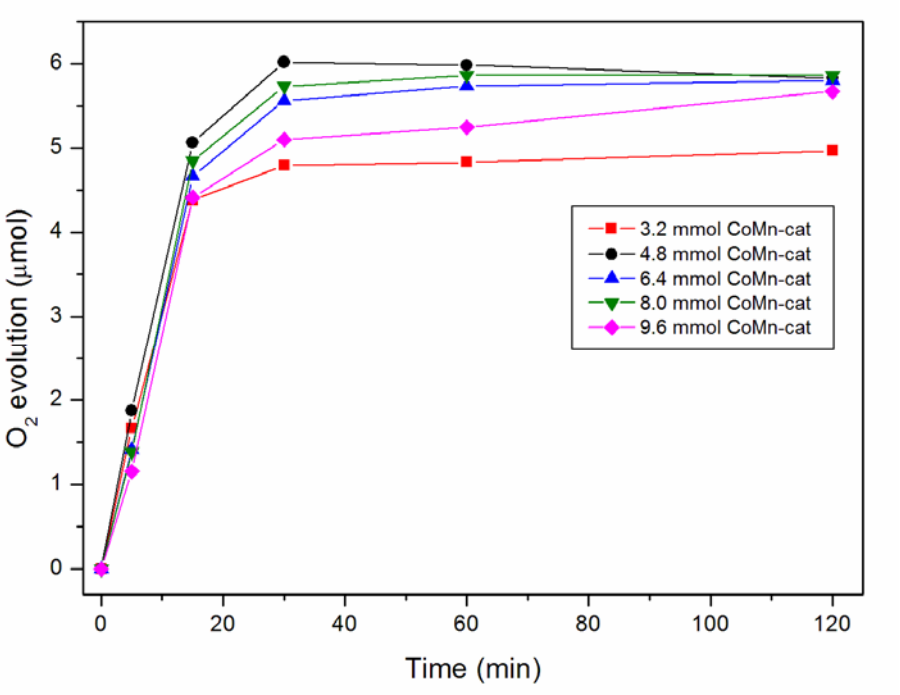

Figure S17. Concentration-dependent WOC activity of Co-Mn-Ga spinel.